

# Efficient Inference in First Passage Time Models

Sicheng Liu\*    Alexander Fengler†    Michael J. Frank‡  
 Matthew T. Harrison§

## Abstract

First passage time models describe the time it takes for a random process to exit a region of interest and are widely used across various scientific fields. Fast and accurate numerical methods for computing the likelihood function in these models are essential for efficient statistical inference. Specifically, in mathematical psychology, generalized drift diffusion models (GDDMs) are an important class of first passage time models that describe the latent psychological processes underlying simple decision-making scenarios. GDDMs model the joint distribution over choices and response times as the first hitting time of a one-dimensional stochastic differential equation (SDE) to possibly time-varying upper and lower boundaries. They are widely applied to extract parameters associated with distinct cognitive and neural mechanisms. However, current likelihood computation methods struggle with common scenarios where drift rates covary dynamically with exogenous covariates in each trial, such as in the attentional drift diffusion model (aDDM). In this work, we propose a fast and flexible algorithm for computing the likelihood function of GDDMs based on a large class of SDEs satisfying the Cherkasov condition. Our method divides each trial into discrete stages, employs fast analytical results to compute stage-wise densities, and integrates these to compute the overall trial-wise likelihood. Numerical examples demonstrate that our method not only yields accurate likelihood evaluations for efficient statistical inference, but also significantly outperforms existing approaches in terms of speed.

**Keywords**— first passage time, first hitting time, drift diffusion model, attention, likelihood-based inference, numerical methods, Cherkasov condition

---

\*Division of Applied Mathematics, Brown University. Email: [sicheng\\_liu@brown.edu](mailto:sicheng_liu@brown.edu)

†Department of Cognitive and Psychological Sciences, Brown University. Email: [alexander\\_fengler@brown.edu](mailto:alexander_fengler@brown.edu)

‡Department of Cognitive and Psychological Sciences, Brown University; Carney Institute for Brain Science, Brown University. Email: [michael\\_frank@brown.edu](mailto:michael_frank@brown.edu)

§Division of Applied Mathematics, Brown University. Email: [matthew\\_harrison@brown.edu](mailto:matthew_harrison@brown.edu)

# 1 Introduction

First passage time models (also known as first hitting time models) are a fundamental class of stochastic process models that describe the time it takes for a random process to exit a region of interest. These models are widely used in various fields, including physics, finance, biology, and cognitive science, to analyze phenomena such as the time until a stock hits a particular price level, the time it takes for a neuron to fire or the time to reach a decision barrier that triggers a choice in psychological experiments [5, 39, 22]. Accurately computing the density of the first passage time is crucial for the practical application of these models, such as in scientific hypothesis testing and parameter estimation. Since analytical solutions for many complex real-world first passage time models are unavailable, effective numerical methods are an indispensable part of the computational toolkit for applying these models. In this paper, we introduce a fast and flexible method for computing the first passage time density in a large class of models arising in cognitive neuroscience, mathematical psychology, and economics.

Consider a psychological experiment in which a subject must choose between two alternatives, A and B. The experimenter records both the choice and the time taken to make it. A common approach to modeling this behavior is through a stochastic process  $X(t)$  that starts at zero and evolves randomly over time until it first reaches  $+a$  or  $-a$ , where  $a$  is the evidence threshold. The choice (A vs. B) is modeled by which boundary is hit ( $+a$  vs.  $-a$ ) and the response time is modeled by the first hitting time.

A widely used model for  $X(t)$  is a Brownian motion with drift

$$X(t) = \mu t + W(t),$$

where  $W(t)$  is a standard Brownian motion. The drift rate  $\mu$  quantifies the strength of the evidence that favors A over B and affects the joint distribution of the choice and the response time. Models such as this are often called **drift diffusion models (DDMs)** [50, 17] and written in differential form, such as,

$$dX(t) = \mu dt + dW(t) \tag{1}$$

with the initial condition  $X(0) = 0$ .

This basic DDM can be modified in a variety of ways to better model experimental data and test theories about the biological processes underlying decision making. For instance, the boundaries ( $\pm a$ ) can be asymmetric and vary over time to reflect changing pressures to make a decision; the starting position  $X(0)$  can be nonzero or random, representing an initial decision bias; the rates of drifting towards the boundaries can depend on the choices and vary over time; and the random process  $X(t)$  can have more complicated stochastic dynamics than Brownian motion [17]. We adopt the terminology from [57] and call these models **generalized drift diffusion models (GDDMs)**. Simple, computationally tractable versions of GDDMs have found widespread use in cognitive neuroscience and mathematical psychology [49, 50, 21, 15, 72]. While more complex versions of

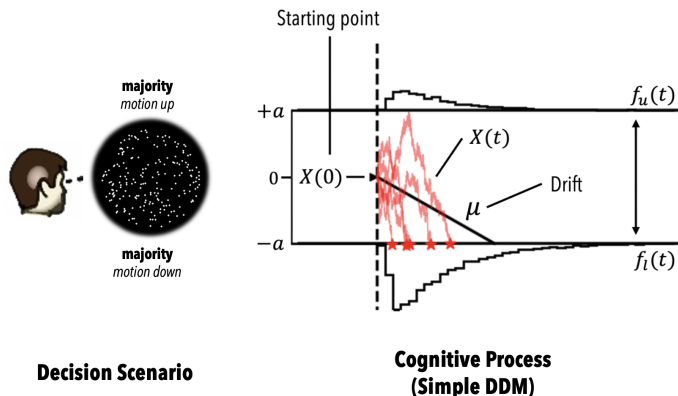


Figure 1: The simple DDM in the context of a canonical experiment in cognitive science, the *dot-motion task*. The DDM serves to represent the *cognitive process* underpinning the choices in this experiment. The task explicitly given to participants: Decide if the majority of dots on the screen are moving up or down. We show trajectories of the corresponding SDE,  $dX(t) = \mu dt + dW(t)$ , in red, and example decision points as *red stars*. The first hitting times distributions  $f_u(t)$ ,  $f_l(t)$  for the corresponding choices (*up*, *down*) are shown above the decision boundaries  $\{+a, -a\}$ .

GDDMs have been proposed to encode a broader range of scientific hypotheses, their quantitative assessment and applications are currently limited due to computational challenges in parameter estimation [17]. In particular, there do not exist fast algorithms for calculating the likelihood function of the parameters (i.e., the probability density of the hitting time on the boundary reached) in some of the more complex GDDMs that are currently of scientific interest.

Computational speed is crucial in many cases for the following reason: The precise specification of the GDDM might change every time a subject makes a choice. An experiment with, say, 50 subjects, each completing 200 trials, might require evaluating the likelihoods of  $10^4$  different versions of the GDDM. For instance, in equation (1) the drift rate  $\mu$  might be different on every trial if the choices presented to subjects are different on every trial. The problem becomes much more difficult when the trial-specific drift rate can vary dynamically within a trial. Our original motivation to study this problem came from **attentional drift diffusion models (aDDMs)** [34], which have been proposed as a model for investigating how visual attention influences decision making. In aDDMs, the drift rate  $\mu(t)$  in each trial is allowed to covary on a moment-by-moment basis, depending on the subject's eye movements toward one choice option or another, which are also recorded in the experimental setup. The entire shape of  $\mu(t)$  changes dramatically on every trial. This model is a generic example of the general class of GDDMs where instantaneous within-trial dynamics can be based on exogenous covariates such as brain activity or eye gaze position, hence

complicating the numerical procedures for computing the first passage time density and further applications. Furthermore, hierarchical Bayesian inference is commonly used in cognitive science to estimate both group- and subject-level parameters simultaneously [70, 17]. The reliance on Markov chain Monte Carlo (MCMC) methods in this context further amplifies the demand for fast likelihood evaluations.

In this paper we introduce fast algorithms for accurately approximating the probability density of the hitting time in a class of GDDMs that have continuous lower and upper boundaries,  $\ell(t)$  and  $u(t)$ , and with dynamics that satisfy the Itô’s stochastic differential equation (SDE)

$$dX(t) = \mu(X(t), t) dt + \sigma(X(t), t) dW(t) \quad (2)$$

for possibly random  $X(0)$  and for functions  $\mu$  and  $\sigma$  satisfying the so-called Cherkasov condition [10, 53]. Loosely speaking, the Cherkasov condition means that the complicated SDE in equation (2) can be transformed into a simpler SDE more akin to equation (1). A special case that includes many cases of practical interest, such as the aDDM, is when  $\mu$  and  $\sigma$  depend only on  $t$  and not on  $X(t)$ <sup>1</sup>. There exist numerical approaches and software for approximating hitting time densities in models even more general than equation (2), but in many cases they are currently too slow for practical use in real-world psychological experiments.

Our approach is closely related to the methods in [67, 42, 47, 68, 60] which approximate the cumulative distribution function of  $X(T)$  at a fixed time  $T$  given that the process has not reached the boundary before  $T$ . Both their method and ours transform the problem into a canonical representation, subdivide time into discrete stages that allow for analytic approximations, compute the final approximation through integration over these stages, and then map the result back to the original problem. However, our work is distinct in that we focus on computing the density of the hitting time rather than the distribution of the process at a fixed time. Additionally, our approach is significantly more computationally efficient, as we pay careful attention to computational details, such as the method of numerical integration. Each of these innovations is crucial for practical likelihood-based inference in modern experimental settings.

The remainder of this article is structured in the following way. Section 2 begins with a mathematical description of the GDDM. Section 3 summarizes previous work related to this paper, including other efforts to address the computational challenges in first passage time models. In Section 4, we introduce our proposed method for computing the FPTDs of certain GDDMs, starting with analytical results for simple DDMs, then combining them sequentially based on Markovian properties. We also apply variable transformations and piecewise linear approximations to extend the method to more complex GDDMs, including those that allow for position-dependent leak and dynamic

---

<sup>1</sup>In the cognitive science context, the terminology “DDM” is typically adopted to denote these models that directly integrate noisy accumulating evidence. The more general model in equation (2), including some examples shown later in this paper (e.g., the Ornstein-Uhlenbeck model), fall within the GDDM framework.

decision boundaries [64, 17]. Section 5 shows several numerical examples that demonstrate the speed and accuracy of our method for both likelihood computation and statistical inference tasks. Section 6 summarizes the conclusion of the present work, including its applicability and suggestions for future work. It is worth mentioning that while our examples are drawn from cognitive science and mathematical psychology, the method we propose is equally applicable to first passage time models in other fields. For instance, it could be extended to financial applications such as pricing double barrier options [36], as well as other areas where first passage times play a critical role.

## 2 Drift Diffusion Model

Here we present a mathematical description of GDDMs. Let  $W(t)$  be a one-dimensional standard Brownian motion and let  $X(t)$  be a (weak) solution of the Itô's stochastic differential equation (SDE) in equation (2) associated with  $W(t)$ , where  $X(0)$  is independent of  $W$ . Let  $u(t)$  and  $\ell(t)$  be two continuous functions representing the upper and lower boundaries, respectively, satisfying  $\mathbb{P}(\ell(0) < X(0) < u(0)) = 1$  and  $\ell(t) \leq u(t)$  for all  $t > 0$ .

In this setting, we aim to study the joint distribution of the first exit time of  $X(t)$  from the time-dependent region  $(\ell(t), u(t))$  and the specific boundary exited (i.e., which choice is made). The first exit time is denoted as  $\tau = \inf\{t > 0 : X(t) \notin (\ell(t), u(t))\}$ , and the boundary hit is denoted as  $C$ , which takes values in the symbol set  $\{u, \ell\}$  to represent which boundary is hit. The event of  $X(t)$  hitting the boundary  $C$  at time  $\tau$  models the participant's decision to choose option  $C$  at time  $\tau$ . The event  $\{\tau = \infty\}$  can never be observed in practice, so we do not explicitly discuss it below. If  $\mathbb{P}(\tau = \infty) > 0$ , then the probability density functions of  $\tau$  discussed in this paper are technically sub-probability density functions that integrate to  $\mathbb{P}(\tau < \infty) < 1$ . This does not affect any of the calculations needed for likelihood-based inference.

We denote the sub-probability density functions

$$f_u(t) = \frac{d}{dt} \mathbb{P}(\tau \leq t, C = u)$$

$$f_\ell(t) = \frac{d}{dt} \mathbb{P}(\tau \leq t, C = \ell)$$

as the first passage time densities (FPTDs) on the upper boundary and lower boundary<sup>2</sup>, respectively, implicitly assuming throughout sufficient regularity conditions on the model for these densities to exist (see the sufficient conditions for density existence in [20, 61]). The marginal density of  $\tau$  is thus given by  $\frac{d}{dt} \mathbb{P}(\tau \leq t) = f_u(t) + f_\ell(t)$ . With this notation, we can write the joint

---

<sup>2</sup>Note that “first passage time density on the upper (lower) boundary” is sometimes interpreted as the density of  $\tau_u = \inf\{t > 0 : X(t) \geq u(t)\}$  ( $\tau_\ell = \inf\{t > 0 : X(t) \leq \ell(t)\}$ ) when only considering one upper boundary  $u(t)$  (lower boundary  $\ell(t)$ ). In this case  $\tau = \tau_u \wedge \tau_\ell$ . These quantities represent different aspects compared to our definition of the FPTD on the upper and lower boundaries and should not be confused.

probability density of  $(\tau, C)$  as

$$f(t, c) = f_u(t)\mathbb{1}_{\{u\}}(c) + f_\ell(t)\mathbb{1}_{\{\ell\}}(c), \quad (3)$$

where  $\mathbb{1}_E(\omega)$  is the indicator function of  $E$  that is 1 if  $\omega \in E$  and 0 otherwise.

If we consider the possible truncation of the process at  $t = T < \infty$ , the process can either exit through the upper boundary  $u(t)$  before  $T$ , exit through the lower boundary  $\ell(t)$  before  $T$ , or fail to hit either boundary by  $T$  and instead reach the truncation boundary  $t = T$ , resulting in three sub-probability densities:

- $f_u(t)\mathbb{1}_{(0, T]}(t)$ : the FPTD on the upper boundary  $u(t)$ , truncated at  $t = T$ .
- $f_\ell(t)\mathbb{1}_{(0, T]}(t)$ : the FPTD on the lower boundary  $\ell(t)$ , truncated at  $t = T$ .
- $q(x) = \frac{d}{dx}\mathbb{P}(X(T) \leq x, \tau > T)$ : the density of the process's position at time  $T$ , provided that it has not hit either upper or lower boundary yet. We refer to  $q$  as the non-passage density (NPD) at  $T$ .

By the conservation of total probability we always have

$$\int_0^T f_u(t) dt + \int_0^T f_\ell(t) dt + \int_{\ell(T)}^{u(T)} q(x) dx = 1$$

for any  $T > 0$ . Define the non-passage probability (NPP) at  $T$  to be

$$Q = \mathbb{P}(\tau > T) = \int_{\ell(T)}^{u(T)} q(x) dx. \quad (4)$$

$Q$  is useful in settings where the process is artificially stopped whenever  $\tau > T$ . For instance, in some psychological experiments, subjects may be required to respond within a certain amount of time  $T$ , otherwise the trial ends with the outcome “non-response” and the NPP  $Q$  is the probability of non-response.

The goal of this paper is to obtain a fast and accurate numerical approximation of the joint density  $f(t, c)$  in equation (3) and the NPP  $Q$  in equation (4). To this end, we develop fast numerical approximations of FPTDs and NPDs, the latter of which are needed for intermediate calculations in our approach.

As mentioned in the Introduction, we are motivated by practical problems for which we need to evaluate many *different* joint densities, each at perhaps a single point. Define  $\Xi = \{\mu(\cdot), \sigma(\cdot), u(\cdot), \ell(\cdot), q_0(\cdot)\}$  to be the configuration of a GDDM, where  $q_0$  is a representation for the distribution of  $X(0)$ , usually a probability density function or a point mass at a deterministic starting point  $x_0$ . In statistical applications,  $\Xi$  will depend on unknown parameters and known covariates, some of which might vary with each trial. If the  $i$ -th trial results in the observation  $(\tau_i, C_i)$ , then the contribution to the likelihood for that trial is  $f(\tau_i, C_i \mid \Xi_i)$ . This is simply the FPTD on the boundary  $C_i$  evaluated at time  $\tau_i$  using the GDDM configuration  $\Xi_i$  for the  $i$ -th trial. In experiments with a time limit, some trials might result in non-response, in which case the

contribution to the likelihood is the NPP for that GDDM configuration, say  $Q_{\Xi_i}$ . A usual experiment in the psychological and cognitive sciences, where GDDMs are ubiquitously applied, produces a dataset with thousands or tens of thousands of trials (across multiple subjects). Consequently, fast and accurate methods for evaluating FPTDs and NPPs are crucial for the practical use of likelihood-based inference in these models.

### 3 Related Work

We briefly review some commonly used computational methods for calculating the density or distribution of first passage times in GDDMs.

**Analytical formulas.** For certain simple DDMs, analytical formulas for the first passage time densities or distributions can be derived, often in the form of infinite series. These methods are fast and accurate, but are typically applicable only for very specific cases. For example, they are available for the standard DDM where all parameters  $\mu, \sigma, x_0, u, \ell$  are constant [41, 6, 26]. The approach in this paper is based on numerically extending these fast special cases to much broader classes of GDDMs. We note that the methods mentioned in the Section 1 for computing distributions [67, 42, 47, 68] can also be used to derive densities by numerically differentiating the distribution. However, the use of finite difference will introduce additional numerical error.

**Numerical solutions of governing equations.** These methods exploit the known connections between diffusion processes and partial differential equations (PDEs), called Kolmogorov equations (see the Chapter 8 of [69] for an introduction, and Chapter 5.7 of [32] for a mathematically rigorous treatment). Both the Kolmogorov forward equation (KFE, also known as Fokker-Planck equation in physics) [57, 13] and the Kolmogorov backward equation (KBE) [66, 65] have been exploited to derive the FPTDs. Moreover, the first passage time problem can be formulated into Volterra integral equations of renewal type [58, 46], where applications to DDMs [59, 43] have also been explored. In these works, numerical methods, particularly finite difference methods [62] due to their simplicity, have been developed to solve these equations, enabling the efficient computation of FPTDs in certain cases. Other numerical methods like discontinuous Galerkin methods have also been considered, see [45] and references therein. However, these approaches remain computationally expensive, especially in settings where the GDDM configuration differs across trials, including but not limited to cases with trial-specific covariates that vary dynamically over time. For a comprehensive review of these methods, we refer the readers to [54].

**Monte Carlo methods.** Monte Carlo methods [24, 31, 25], including exact simulation methods [29, 30], generally require large sample sizes to ensure accurate likelihood approximations, making them slow in practice. However, we apply Monte Carlo methods in Section 5 to verify the results of our approach. The simulation results can support statistical inference by enabling the comparison of summary statistics between observed and simulated data [51]. Methods

such as density estimation [14] and approximate Bayesian computation (ABC) [55, 3] are commonly employed for this purpose.

**Simulation Based Inference (SBI).** Another alternative approach, which is gaining traction in recent years, is to train machine learning models on simulated data as a surrogate for likelihoods. The surrogate likelihood function is commonly represented by a neural network [44, 18, 48, 7, 27] or a Gaussian process [1, 71]. This allows the expensive Monte Carlo simulations to be carried out prior to data collection. The inexpensive amortized likelihoods can be deployed at inference time to speed up parameter estimation [11, 18]. However, for cases where  $\Xi$  has high-dimensional parameters or covariates that dynamically vary in time, the amortization becomes cumbersome or intractable. Another current drawback of SBI is that the user has less control over the quality of the resulting approximations. We are not aware of any SBI work specifically applied to the specific models highlighted in this paper. However, we mention SBI as a promising general purpose alternative, which in principle can have bearing on the model domain under discussion in this work.

## 4 Main Methods

In this section, we present our main algorithm for computing FPTDs and NPDs. We begin by studying a simple case where analytical results are known in Section 4.1 then generalize it to more complicated cases in Sections 4.2–4.5.

### 4.1 Single-stage Model

We consider the Brownian motion with drift

$$dX(t) = \mu dt + \sigma dW(t) \quad (5)$$

starting at  $x_0$ . There are two linear absorbing boundaries

$$\text{upper: } u(t) = a_1 + b_1 t, \quad \text{lower: } \ell(t) = a_2 + b_2 t$$

with  $a_2 < x_0 < a_1$ , and, additionally, a truncation boundary at  $t = T$  such that  $\ell(t) < u(t)$  on  $[0, T]$ . We name this the “**single-stage model**” as it is the building block of our method.

[28] derives the following analytical formulas<sup>3</sup> for FPTDs and NPDs in the single-stage model for the special case when  $x_0 = 0$  and  $\sigma = 1$ : We define  $\bar{a} = \frac{a_1 + a_2}{2}$ ,  $\bar{b} = \frac{b_1 + b_2}{2}$ ,  $c = a_1 - a_2$ ,  $b = \frac{b_2 - b_1}{2}$ , then

- The FPTD on the upper boundary  $u(t)$  is given by

$$f_u^{\text{basic}}(t; \mu, a_1, b_1, a_2, b_2, T) = \frac{1}{\sqrt{2\pi t^3}} e^{-\frac{b}{c} a_1^2 + a_1 \delta_u - \frac{1}{2} \delta_u^2 t} \sum_{j=0}^{\infty} (-1)^j \alpha_j e^{(\frac{b}{c} - \frac{1}{2t}) \alpha_j^2} \mathbb{1}_{(0, T]}(t) \quad (6)$$

<sup>3</sup>Another work along this direction is [2]. We adopt the results in [28] since they are simpler and were shown to agree with those of [2]. Equation (9), (10), and (11) have been slightly rewritten for use in this paper, compared to their original form in [28].



where  $\delta_u = \mu - b_1$ ,  $\alpha_j = (j + \frac{1}{2})c + (-1)^j \bar{a}$ .

- Similarly, the FPTD on the lower boundary  $\ell(t)$  is given by

$$f_\ell^{\text{basic}}(t; \mu, a_1, b_1, a_2, b_2, T) = \frac{1}{\sqrt{2\pi t^3}} e^{-\frac{b}{c} a_2^2 - a_2 \delta_\ell - \frac{1}{2} \delta_\ell^2 t} \sum_{j=0}^{\infty} (-1)^j \beta_j e^{(\frac{b}{c} - \frac{1}{2t}) \beta_j^2} \mathbb{1}_{(0, T]}(t) \quad (7)$$

where  $\delta_\ell = -\mu + b_2$ ,  $\beta_j = (j + \frac{1}{2})c - (-1)^j \bar{a}$ .

- Letting  $y = x - \bar{b}T$ , the NPD at the vertical boundary  $t = T$  is given by

$$q^{\text{basic}}(x; \mu, a_1, b_1, a_2, b_2, T) = \frac{1}{\sqrt{2\pi T}} e^{(\mu - \bar{b})x - \frac{1}{2}(\mu^2 - \bar{b}^2)T} \left\{ e^{-\frac{y^2}{2T}} + \sum_{j=1}^{\infty} \left[ e^{4bj(jc - \bar{a}) - \frac{(y - 2jc)^2}{2T}} - e^{2b(2j-1)(jc - a_1) - \frac{(y + 2jc - 2a_1)^2}{2T}} + e^{4bj(jc + \bar{a}) - \frac{(y + 2jc)^2}{2T}} - e^{2b(2j-1)(jc + a_2) - \frac{(y - 2jc - 2a_2)^2}{2T}} \right] \right\} \mathbb{1}_{(\ell(T), u(T))}(x) \quad (8)$$

For the single-stage model (5) with a nonzero starting point  $x_0$  and a diffusion coefficient  $\sigma$  that does not equal to 1, it's straightforward to obtain its FPTDs and NPD by some shifting and scaling: For notational convenience we further let  $\mathcal{B} = (a_1, b_1, a_2, b_2, T)$  denote the collection of all the boundary parameters, then we have

$$f_u^{\text{single}}(t; \mu, \sigma, \mathcal{B}, x_0) = f_u^{\text{basic}}\left(t; \frac{\mu}{\sigma}, \frac{a_1 - x_0}{\sigma}, \frac{b_1}{\sigma}, \frac{a_2 - x_0}{\sigma}, \frac{b_2}{\sigma}, T\right) \quad (9)$$

$$f_\ell^{\text{single}}(t; \mu, \sigma, \mathcal{B}, x_0) = f_\ell^{\text{basic}}\left(t; \frac{\mu}{\sigma}, \frac{a_1 - x_0}{\sigma}, \frac{b_1}{\sigma}, \frac{a_2 - x_0}{\sigma}, \frac{b_2}{\sigma}, T\right) \quad (10)$$

$$q^{\text{single}}(x; \mu, \sigma, \mathcal{B}, x_0) = \frac{1}{\sigma} q^{\text{basic}}\left(\frac{x - x_0}{\sigma}; \frac{\mu}{\sigma}, \frac{a_1 - x_0}{\sigma}, \frac{b_1}{\sigma}, \frac{a_2 - x_0}{\sigma}, \frac{b_2}{\sigma}, T\right) \quad (11)$$

An illustration of the single-stage model is shown in Figure 2(a).

## 4.2 Integrated Single-stage Model

The single-stage model uses  $X(0) = x_0$  deterministically. If, instead,  $X(0)$  is random, then the corresponding FPTDs and NPDs can be obtained by taking the expectations of (9), (10), and (11) over the distribution of  $X(0)$ . We call this the **integrated single-stage model**. If the distribution of  $X(0)$  has a probability density function  $q_0$  supported on  $(a_2, a_1)$ , then FPTDs and NPDs

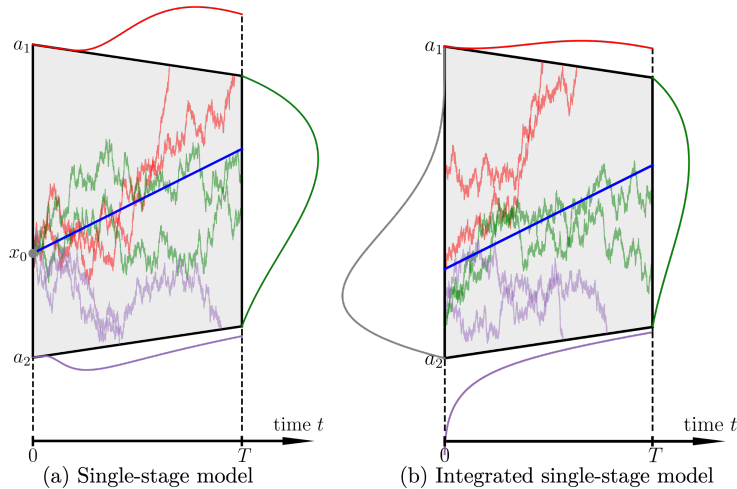


Figure 2: (a) A single-stage model is a GDDM with constant drift  $\mu$  and two linear boundaries  $u(t), \ell(t)$  starting at  $x = x_0$  and truncated at  $t = T$ . The process can hit one of  $u(t)$  and  $\ell(t)$  before  $T$ , or hit neither. This results in three distinct subprobability distributions, corresponding to these three outcomes, with their subprobability densities plotted by red, purple, and green curves along the boundaries. Sample trajectories, colored to match their respective outcomes, are also displayed. The blue line represents the expected value of the process, given by  $\mathbb{E}[X(t)] = x_0 + \mu t$ . In a single-stage model the total area under the three subprobability density curves sums to 1. (b) The integrated single-stage model extends the single-stage model by introducing random variability in the initial position  $X(0)$ . The expected value of the process in this model is given by  $\mathbb{E}[X(t)] = \mathbb{E}[X(0)] + \mu t$ , represented by the blue line. The density of  $X(0)$ , denoted by  $q_0$ , is illustrated by the grey curve. We allow  $q_0$  to be a subprobability density function. In an integrated single-stage model, the total area under the three outcome subprobability density curves sums to the area under the initial grey curve.

for the integrated single-stage model are

$$\begin{aligned}
 f_u^{\text{int}}(t; \mu, \sigma, \mathcal{B}, q_0) &= \int_{a_2}^{a_1} f_u^{\text{single}}(t; \mu, \sigma, \mathcal{B}, x_0) q_0(x_0) dx_0, \\
 f_\ell^{\text{int}}(t; \mu, \sigma, \mathcal{B}, q_0) &= \int_{a_2}^{a_1} f_\ell^{\text{single}}(t; \mu, \sigma, \mathcal{B}, x_0) q_0(x_0) dx_0, \\
 q^{\text{int}}(x; \mu, \sigma, \mathcal{B}, q_0) &= \int_{a_2}^{a_1} q^{\text{single}}(x; \mu, \sigma, \mathcal{B}, x_0) q_0(x_0) dx_0.
 \end{aligned} \tag{12}$$

An illustration of the integrated single-stage model is shown in Figure 2(b).

Below, we use the same definitions and formulas in equation (12) when  $q_0$  is a sub-probability density function. This usage forms the basis of our

multi-stage model below. When  $X(0)$  is a discrete random variable, we abuse notation and allow  $q_0 = \sum_{j=1}^J w_{0j} \delta_{x_{0j}}$  to be a weighted sum of point masses, where  $(w_{01}, \dots, w_{0J})$  is a probability mass function on  $(x_{01}, \dots, x_{0J})$  and  $\delta$  is the Dirac delta generalized function. For instance, when  $q_0 = \delta_{x_0}$  we have  $f_u^{\text{int}}(t; \mu, \sigma, \mathcal{B}, q_0) = f_u^{\text{single}}(t; \mu, \sigma, \mathcal{B}, x_0)$  and similarly for  $f_\ell^{\text{int}}$  and  $q^{\text{int}}$ , so that a single-stage model can be viewed as a special case of the integrated single-stage model.

### 4.3 Multi-stage Model

We define **multi-stage models** to be GDDMs with piecewise constant drift coefficient, piecewise constant diffusion coefficient, and continuous piecewise linear boundaries, which can be divided at their segment points such that each stage reduces to an integrated single-stage model. To be specific, a  $d$ -stage model is a stochastic process

$$dX(t) = \mu(t) dt + \sigma(t) dW(t)$$

stopped by a continuous piecewise linear upper boundary  $u(t)$ , a continuous piecewise linear lower boundary  $\ell(t)$  and a vertical boundary  $t = T_{\text{end}}$ , where  $\mu(t)$  is a piecewise constant drift function and  $\sigma(t)$  is a piecewise constant diffusion function. Let  $0 < t_1 < \dots < t_{d-1} < T_{\text{end}}$  be the  $d-1$  segment points for  $\mu(t), \sigma(t), u(t)$  and  $\ell(t)$  prior to  $T_{\text{end}}$ , and define  $t_0 = 0$  and  $t_d = T_{\text{end}}$ . Then  $\mu(t), \sigma(t), u(t)$  and  $\ell(t)$  can be defined as

$$\left. \begin{aligned} \mu(t) &= \mu_k \\ \sigma(t) &= \sigma_k \\ u(t) &= a_{k1} + b_{k1}(t - t_{k-1}) \\ \ell(t) &= a_{k2} + b_{k2}(t - t_{k-1}) \end{aligned} \right\} \text{when } t_{k-1} < t \leq t_k$$

for  $1 \leq k \leq d$ . Note that we must have  $a_{k1} + b_{k1}(t_k - t_{k-1}) = a_{k+1,1}$  and  $a_{k2} + b_{k2}(t_k - t_{k-1}) = a_{k+1,2}$  for  $1 \leq k \leq d-1$  to ensure the continuity of  $u(t)$  and  $\ell(t)$ . We denote the process during time interval  $(t_{k-1}, t_k]$  to be the  $k$ -th (integrated single) stage, which has a drift coefficient  $\mu_k$ , diffusion coefficient  $\sigma_k$ , and boundary parameters  $\mathcal{B}_k = (a_{k1}, b_{k1}, a_{k2}, b_{k2}, T_k = t_k - t_{k-1})$ , for  $1 \leq k \leq d$ . By the Markov property, the NPD  $q^{\text{int}}$  in equation (12) from the  $(k-1)$ -st stage becomes the initial position density  $q_0$  of the  $k$ -th stage. Since the process could have hit the upper or lower boundary in an earlier stage, the NPD is a sub-probability density function, which is why we allowed  $q_0$  to be a sub-probability density function in the definition of the integrated single-stage model.

To compute the FPTDs and NPDs of a multi-stage model, we first divide the multi-stage model into several integrated single-stage models and then proceed sequentially: For the first stage, the initial position  $X(0)$  has the same distribution as that of the considered multi-stage model (deterministic or random). Starting from the second stage, the NPD from the previous stage becomes the initial position distribution of the current stage. The FPTDs of each stage

correspond exactly to the FPTDs of the original multi-stage model over the corresponding time interval. An illustration of the sequential computation is presented in Figure 3. In settings with the possibility of non-response before  $T_{\text{end}}$ , we can also compute the NPP  $Q$  at  $T_{\text{end}}$  by integrating the final NPD. Specifically, recalling that the density of  $\tau$  on the upper and lower boundaries is denoted as  $f_u(t)$  and  $f_\ell(t)$ , respectively, then we can write the whole sequential algorithm as Algorithm 1. A formal derivation of the validity of the algorithm uses the Markov property and the Chapman-Kolmogorov equation with each single-stage model behaving like a sub-probability Markov transition kernel from one stage boundary to the next. We give a concrete example illustrating the complete computation process of applying Algorithm 1 to a multi-stage model in Figure 4.

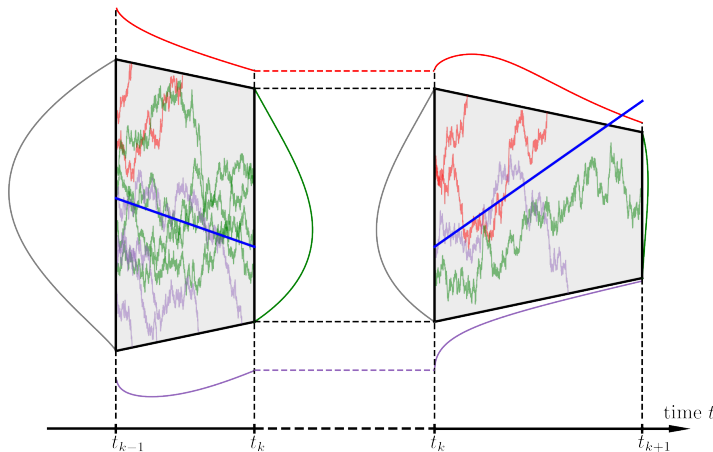


Figure 3: An illustration of the sequential computation from the  $k$ -th stage to the  $(k+1)$ -th stage in a multi-stage model. The  $k$ -th stage (depicted on the left side of the figure) is an integrated single-stage model, where the density of its starting position is given by  $q_{k-1}(x)$  (represented by the grey curve). Within this stage, the functions  $f_u(t)\mathbb{1}_{(t_{k-1}, t_k]}(t)$  (red curve),  $f_\ell(t)\mathbb{1}_{(t_{k-1}, t_k]}(t)$  (purple curve), and  $q_k(x)$  (green curve) are obtained by integrating the formulas (9), (10), and (11) over  $q_{k-1}$ , respectively. The resulting NPD  $q_k(x)$  then serves as the starting position distribution for the  $(k+1)$ -th stage, facilitating the subsequent computation (depicted on the right side of the figure).

For multi-stage models, Algorithm 1 is exact in the sense that the only error is the numerical error. We note, however, that equations (6) and (7) are singular at  $t = 0$ , which can lead to numerical instability in Algorithm 1 if the observation time  $t \in (t_{k-1}, t_k]$  is very close to  $t_{k-1}$ . In practical scenarios, this issue can usually be avoided via data post-processing that slightly inflates the value of any  $t$  that happens too close to the beginning of a stage. This will have negligible impact on parameter estimation, particularly in cognitive psychology

---

**Algorithm 1:** Sequential likelihood evaluation of a multi-stage GDDM
 

---

**Input** : A multi-stage model configuration as described in Section 4.3.

An observation  $(t, c)$  for  $0 < t \leq T_{\text{end}}$  and  $c \in \{u, \ell\}$  or an observation of “non-response”.

**Output:**  $f(t, c) = f_c(t)$  for a datum pair  $(t, c)$ , or  $Q$  for “non-response”

**for**  $k = 1$  **to**  $d$  **do**

$$\left. \begin{aligned} f_u(t) &= f_u^{\text{int}}(t - t_{k-1}; \mu_k, \sigma_k, \mathcal{B}_k, q_{k-1}) \\ f_\ell(t) &= f_\ell^{\text{int}}(t - t_{k-1}; \mu_k, \sigma_k, \mathcal{B}_k, q_{k-1}) \end{aligned} \right\} \text{ for } t \in (t_{k-1}, t_k]$$

$$q_k(x) = q^{\text{int}}(x; \mu_k, \sigma_k, \mathcal{B}_k, q_{k-1}) \text{ for all } x \in (\ell(t_k), u(t_k))$$

**end**

$$Q = \int_{\ell(t_d)}^{u(t_d)} q_d(x) dx$$


---

applications where any numerical corrections are going to lie well within the measurement error of participant reaction times.

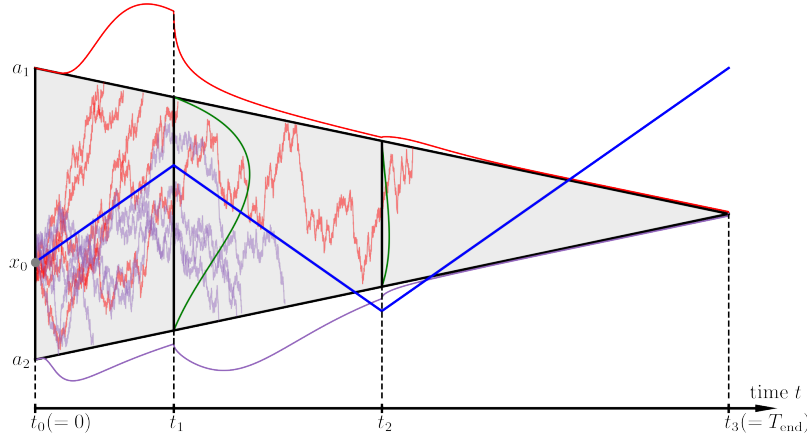


Figure 4: Example of applying the multi-stage algorithm to a GDDM with drift term  $\mu_1 \mathbb{1}_{[0, t_1) \cup [t_2, \infty)}(t) + \mu_2 \mathbb{1}_{[t_1, t_2)}(t)$ , constant  $\sigma$  and linearly collapsing boundaries that collapse at  $t_3$ . The process is divided into 3 single-stage models according to  $t \in [0, t_1), [t_1, t_2), [t_2, t_3)$ . The FPTDs can be computed sequentially from the early to the late stages, and are plotted along their respective boundaries. Example trajectories are shown with different colors representing which boundary the trajectory first hits (red indicates upper boundary, purple indicates lower).

## 4.4 Approximating with the Multi-stage Model

For GDDMs of the same form as the multi-stage model, but with boundaries that are not piecewise linear, it is natural to consider approximating the GDDM with a multi-stage model by approximating the boundaries  $u(t)$  and  $\ell(t)$  with continuous piecewise linear functions. Choosing time points  $0 = t_0 < t_1 < \dots < t_d = T_{\text{end}}$  that include any times when  $\mu(t)$  or  $\sigma(t)$  changes values, we can define  $\bar{u}(t)$  and  $\bar{\ell}(t)$  to be the continuous piecewise linear functions that are linear on each interval  $(t_{k-1}, t_k]$  and for which  $\bar{u}(t_k) = u(t_k)$  and  $\bar{\ell}(t_k) = \ell(t_k)$  for each  $k$ . The original process with these new boundaries gives a multi-stage model that approximates the original GDDM. The FPTDs and NPDs of the approximating multi-stage model can be computed with Algorithm 1 and used as approximations of the FPTDs and NPDs for the original GDDM.

Define  $\bar{\tau} = \inf\{t > 0 : X(t) \notin (\bar{\ell}(t), \bar{u}(t))\}$  to be the hitting time of the process to the approximating boundaries. As the approximation gets increasingly fine, meaning  $\max_k |t_k - t_{k-1}| \rightarrow 0$ , then it is straightforward to show that  $\bar{\tau} \rightarrow \tau$  with probability one under mild regularity conditions on the boundaries (see the proof in Appendix A). Showing that the FPTDs also converge is beyond the scope of this paper and presumably requires additional regularity assumptions on the boundaries, such as continuous differentiability. We provide empirical evidence in the examples below that this method of approximation works well.

## 4.5 Transformations

For GDDMs that cannot be directly approximated with a multi-stage model as in Section 4.4, a transformation into an equivalent GDDM that is amenable to approximation may be possible.

Consider a transform  $(t, x) \mapsto (s, w)$  defined as

$$\begin{aligned} s &= \gamma(t) \\ w &= \psi(x, t) \end{aligned} \tag{13}$$

for  $t \geq 0$ ,  $x \in \mathbb{R}$ , where  $\gamma : [0, \infty) \rightarrow [0, D)$  is one-to-one, increasing, and differentiable with derivative  $\gamma'$  for some  $0 < D \leq \infty$ ,  $\psi : \mathbb{R} \times [0, \infty) \rightarrow \mathbb{R}$  is continuous, and for each  $t \geq 0$ ,  $\psi(\cdot, t) : \mathbb{R} \rightarrow \mathbb{R}$  is one-to-one, increasing, and differentiable with derivative  $\psi'(\cdot, t)$  and inverse  $\psi^{-1}(\cdot, t)$ . The GDDM in the new coordinate system is

$$\begin{aligned} \tilde{X}(s) &= \psi(X(\gamma^{-1}(s)), \gamma^{-1}(s)), \\ \tilde{u}(s) &= \psi(u(\gamma^{-1}(s)), \gamma^{-1}(s)), \\ \tilde{\ell}(s) &= \psi(\ell(\gamma^{-1}(s)), \gamma^{-1}(s)), \\ \tilde{\tau} &= \inf\{s > 0 : \tilde{X}(s) \notin (\tilde{\ell}(s), \tilde{u}(s))\}, \\ \tilde{C} &= \text{exiting boundary} \in \{u, \ell\} \end{aligned}$$

with the distribution of  $\tilde{X}(0) = \psi(X(0), 0)$  defined by the distribution of  $X(0)$ . If  $X(0)$  has density  $q_0$ , then  $\tilde{X}(0)$  has density  $\tilde{q}_0(x) = q_0(\psi^{-1}(x, 0))/\psi'(\psi^{-1}(x, 0))$ .

The assumptions on  $\gamma$  and  $\psi$  ensure that  $\tilde{u}$  and  $\tilde{\ell}$  are continuous and that

$$\tilde{\tau} = \gamma(\tau) \quad \text{and} \quad \tilde{C} = C.$$

Hence, the FPTDs  $f_c$  of  $X$  are related to the FPTDs  $\tilde{f}_c$  of  $\tilde{X}$  via

$$f_c(t) = \frac{d}{dt} \mathbb{P}(\tau \leq t, C = c) = \frac{d}{dt} \mathbb{P}(\tilde{\tau} \leq \gamma(t), \tilde{C} = c) = \gamma'(t) \tilde{f}_c(\gamma(t)) \quad (14)$$

for  $c \in \{u, \ell\}$ , and the NPD  $q$  of  $X$  at  $T$  is related to the NPD  $\tilde{q}$  of  $\tilde{X}$  at  $\gamma(T)$  via

$$\begin{aligned} q(x) &= \frac{d}{dx} \mathbb{P}(X(T) \leq x, \tau > T) = \frac{d}{dx} \mathbb{P}(\tilde{X}(\gamma(T)) \leq \psi(x, T), \tilde{\tau} > \gamma(T)) \\ &= \psi'(x, T) \tilde{q}(\psi(x, T)). \end{aligned} \quad (15)$$

The NPP  $Q$  of  $X$  at  $T$  is simply the NPP  $\tilde{Q}$  of  $\tilde{X}$  at  $\gamma(T)$ . Consequently, any method for approximating the FPTDs and NPDs of the transformed GDDM  $\tilde{X}$  can be used to approximate the FPTDs and NPDs of the original GDDM  $X$  using equations (14) and (15). The trick is to find a transformation for which the resulting  $\tilde{X}$  gives a GDDM that is amenable to approximation.

A particularly simple  $\tilde{X}$  is standard Brownian motion, perhaps with a random starting point, i.e., equation (2) with  $\mu(x, t) \equiv 0$  and  $\sigma(x, t) \equiv 1$ . A wide range of commonly used SDEs can be transformed into standard Brownian motion in this way, including geometric Brownian motion, the Ornstein-Uhlenbeck (O-U) process, and the Brownian bridge, among others. The question of whether a diffusion process can be transformed to a Brownian motion through transformation of the type in equation (13) was raised by Kolmogorov in [33]. Cherkasov gave a constructive proof of the necessary and sufficient condition for the existence of such a transformation in [10], which is now commonly referred as the Cherkasov condition in the literature. This was recast into a simpler form in [53], and was later used in [52] to obtain the one-sided first passage time density through the integral equation method. We present the Cherkasov condition in [53] in Appendix B, and instead of focusing on the condition itself, we provide specific examples of the transformation from diffusion processes to Brownian motion that are common in practical applications.

- **DDMs with nonlinear drift.** One simple but important subclass of models that fits this transformation is

$$dX(t) = \mu(t) dt + \sigma dW(t) \quad (16)$$

with possibly nonlinear time-dependent drift term  $\mu(t)$ . The SDE (16) can be solved via a direct integration:

$$X(t) = X(0) + \int_0^t \mu(r) dr + \sigma W(t)$$

and consequently, through transformation  $w = \psi(x, t) = \frac{1}{\sigma}(x - \int_0^t \mu(r) dr)$  (in this case  $s = \gamma(t) = t$ , so we still use  $t$ ) we have

$$\tilde{X}(t) = \psi(X(t), t) = \frac{X(0)}{\sigma} + W(t). \quad (17)$$

The right hand side of (17) is a Brownian motion with initial position  $X(0)/\sigma$ . We illustrate the approximate FPTD computation for this example in Section 5.2.

- **Ornstein-Uhlenbeck model.** The nonstationary Ornstein-Uhlenbeck (O-U) process  $X(t)$  is defined by the following stochastic differential equation:

$$dX(t) = \theta(\lambda - X(t)) dt + \sigma dW(t) \quad (18)$$

where  $\theta \neq 0, \lambda \in \mathbb{R}, \sigma > 0$  are constants. When  $\theta > 0$  it models the “mean-reverting” phenomenon as the process tends towards  $\lambda$  over time, and it will converge to its stationary distribution  $\mathcal{N}(\lambda, \frac{\sigma^2}{2\theta})$  as  $t$  goes to infinity. This model has a long history in cognitive science [64], where it is called the *leaky competing accumulator* model of decision making. This model can flexibly capture evidence accumulation and neural dynamics that are either leaky (for  $\theta < 0$ , such that earlier bits of evidence are disregarded relative to later bits, due to mean reversion), or attractive (for  $\theta > 0$ , where early evidence dominates); see [9].

The solution of (18) is given by [22]

$$X(t) = \lambda + e^{-\theta t}(X(0) - \lambda) + \sigma e^{-\theta t} \int_0^t e^{\theta r} dW(r).$$

The stochastic integral can be viewed as a time-changed Brownian motion [16]:

$$X(t) = \lambda + e^{-\theta t}(X(0) - \lambda) + \sigma e^{-\theta t} \tilde{W}\left(\frac{e^{2\theta t} - 1}{2\theta}\right), \quad (19)$$

where  $\tilde{W}$  is another standard Brownian motion (identical only in distribution to the original  $W$ ). We perform the transformation  $s = \gamma(t) = (e^{2\theta t} - 1)/(2\theta)$  and  $w = \psi(x, t) = (e^{\theta t}x - \lambda e^{\theta t} + \lambda)/\sigma$  so that the transformed process becomes

$$\tilde{X}(s) = \psi(X(\gamma^{-1}(s)), \gamma^{-1}(s)) = \frac{1}{\sigma}X(0) + \tilde{W}(s)$$

which is a Brownian motion with initial position  $X(0)/\sigma$ .

In Section 5.3, we use this transformation and adopt the procedures in this section to compute the FPTDs of the O-U process.

Additionally, for parametric models like the O-U process, we can also study their “multi-stage” versions with piecewise constant parameters, as well as “attentional” versions, where the values of these piecewise constant parameters and



the stage durations are influenced by attention mechanisms. Our Algorithm 1 naturally admits generalization to these models, in which case the breakpoints between stages will contain both the saccade times and the segment points for approximating the nonlinear transformed boundaries.

Even if the original model has simple boundaries, the transformed model could have complicated boundaries that make approximations based on the multi-stage model less accurate or that lead to numerical instabilities. For instance, the time transformation  $s = \gamma(t)$  in the O-U process is exponential and might lead to time dilation issues if one is interested in the FPTDs at large decision times.

## 4.6 Algorithm Summary

The complete process of approximating  $f(t, c)$  and/or  $Q$  is as follows:

- If necessary, use the methods in Section 4.5 to mathematically transform the GDDM into a representation with constant or piecewise constant  $\mu(t)$  and  $\sigma(t)$ .
- If necessary, use the strategy in Section 4.4 to approximate the upper and lower boundaries with piecewise linear functions, so that the approximate model is a multi-stage model.
- Use Algorithm 1 in Section 4.3 to calculate the FPTD or the NPP of the multi-stage model.
- If necessary, use the methods of Section 4.5 to transform the resulting FPTD from the multi-stage model back into the FPTD of the original GDDM.

## 4.7 Fast Implementation

In this section, we discuss some practical aspects of our algorithm that contribute to its fast execution, including important details about numerical integration and function representation that are glossed over in the description of Algorithm 1.

- If we have multiple observations for *the same* GDDM, then one pass of Algorithm 1 can be used to evaluate the likelihood for all observations for this GDDM, thereby eliminating redundant computations.
- If  $t \in (t_{k-1}, t_k]$ , then we can halt Algorithm 1 after the evaluation of  $f_c(t)$  in the  $k$ -th stage. Also, note that evaluations of  $f_u$  and  $f_\ell$  can be skipped unless they are needed for the final output, since only  $q_k$  is propagated across stages.
- To compute the likelihood given a dataset, we simply iterate Algorithm 1 over all data. The computation of each trial in a dataset is independent of

each other, rendering the problem “embarrassingly parallelizable” across trials — we can distribute the dataset over multiple threads, and since no communication is needed between the sub-tasks, the computational time should ideally be inversely proportional to the number of threads.

- Formulas (6), (7) and (8) are approximated by truncating the infinite sum to a desired accuracy. The truncation criteria can be used as a way to balance speed and accuracy. Empirically, we observe that the series usually converge numerically with very few terms.
- All numerical integrations in equation (12) as used by Algorithm 1 are performed with Gauss-Legendre quadrature (see Chapter 5.5 of [56] for an introduction). This approach offers higher accuracy with fewer integrand evaluations compared to alternative methods, such as the trapezoidal rule. We specifically benefit from this in our method because our integrands consist of (truncated) infinite series, which are expensive to evaluate. It also means that each  $q_k$  within the algorithm needs only to be represented at a small number of pre-determined quadrature points. Details of the implementation of Algorithm 1 regarding quadrature are shown in Appendix C.
- Piecewise linear approximations of the transformed boundaries in Section 4.5 are realized via adaptive linear interpolation, which balances accuracy and computational efficiency by dynamically adjusting both the number and position of interpolation points based on the function’s variability.

In our program, we implement the core functionality in Python, with performance-critical parts written using Cython [4], leveraging both the flexibility of Python and the high efficiency of C. OpenMP parallelization is supported to speed up the likelihood computation for large datasets. Our code, along with usage examples—including numerical examples presented in Section 5—will be released as an open-source Python package upon publication for reproducibility. Additionally, our codes will be integrated into the HSSM package [19] for hierarchical Bayesian inference of GDDMs.

## 5 Numerical Examples

In this section, we provide several numerical examples to demonstrate the effectiveness of our method. In Examples 5.1, 5.2, and 5.3, we compute exact or approximate FPTDs using Algorithm 1 and verify the results by comparing them with simulated data. In Section 5.4, we showcase the speed of Algorithm 1 for likelihood computation and statistical inference.

It is worth mentioning that accurately simulating first passage times of stochastic processes is itself a challenging problem (see [63] for a discussion regarding Brownian motion). The usual approach, which we have also adopted, is to discretize the SDE (16) according to the Euler-Maruyama scheme: let

$0 < r_1 < r_2 < \dots$  be a temporal grid, simulate  $\widehat{X}(0)$  according to the distribution of  $X(0)$ , then proceed as

$$\widehat{X}(r_{n+1}) = \widehat{X}(r_n) + \mu(\widehat{X}(r_n), r_n)(r_{n+1} - r_n) + \sigma(\widehat{X}(r_n), r_n)\Delta W(r_n)$$

to simulate an approximate sample path of  $X$ , where the random variable  $\Delta W(r_n) = W(r_{n+1}) - W(r_n)$  is distributed as  $\mathcal{N}(0, r_{n+1} - r_n)$ , and all  $\Delta W(r_n)$ 's are independent. Such simulation will of course be biased due to the unavoidable discretization error. Then, the first passage time data is the first time  $r_n$  such that  $\widehat{X}(r_n) \notin (\ell(r_n), u(r_n))$ . However, even if we could simulate  $X$  exactly on the discrete grid  $\{r_n\}_{n=1}^\infty$ , this would not sample  $\tau$  exactly, as it is possible for  $X$  to cross the barrier between grid points  $r_n$  and  $r_{n+1}$  without exceeding the barrier at either of these grid points.

In our experiment, we simply use a very small step size  $\Delta r = r_{n+1} - r_n = 10^{-5}$  and a large sample size to reduce the approximation error. More advanced techniques, such as Brownian bridge interpolation, are also commonly used to address this issue (see the chapter 6-7 of [23] for a general introduction), however for the purposes of this work, the simulation data serves as a sanity-check more than an object of independent interest.

## 5.1 FPTDs for GDDMs with piecewise Constant Drift

We consider a GDDM with piecewise constant drift

$$\mu(t) = \begin{cases} 1 & 0 < t \leq 1 \\ -0.2 & 1 < t \leq 2.5 \\ 1.5 & 2.5 < t \leq 3.5 \\ 0.5 & 3.5 < t \leq 4 \\ -1 & 4 < t \leq 5 \end{cases}$$

constant diffusion  $\sigma = 1$  and linear collapsing boundaries:

$$u(t) = 1.5 - 0.3t, \quad \ell(t) = -1.5 + 0.3t$$

starting at  $x_0 = -0.5$ . This is a generic example of a multi-stage model. Unlike the aDDM, here the breakpoints of the drift function are the same for all trials.

We use our Algorithm 1 to compute the FPTDs on the upper boundary and lower boundary and compare them with the normalized histogram obtained from 50000 Monte Carlo samples. The results are shown in Figure 5. The FPTD exhibits corners at all breakpoints of  $\mu(t)$ . Despite this complexity, our result visually matches the empirical densities.

## 5.2 FPTDs for GDDMs with Nonlinear Drift and Boundaries

Consider the GDDMs in equation (16) with possibly nonlinear time-dependent drift term  $\mu(t)$  and boundaries  $u(t), \ell(t)$ . Following the transform discussed in

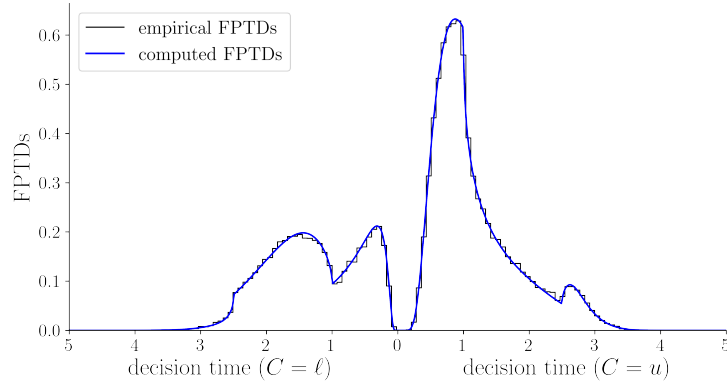


Figure 5: Plots of FPTDs and histogram for Example 5.1: a GDDM with piecewise constant drift. First passage times on the upper boundary are displayed on the positive  $t$ -axis and those on the lower boundary are displayed on the negative  $t$ -axis so that the whole plot is a valid probability density function.

Section 4.5, we can write the transformed boundaries as

$$\tilde{u}(t) = \frac{1}{\sigma} \left( u(t) - \int_0^t \mu(r) dr \right), \quad \tilde{\ell}(t) = \frac{1}{\sigma} \left( \ell(t) - \int_0^t \mu(r) dr \right)$$

and work with the transformed model  $\tilde{X}(t) = \frac{X(0)}{\sigma} + W(t)$ . We approximate  $\tilde{u}(t)$  and  $\tilde{\ell}(t)$  by piecewise linear functions and use Algorithm 1 to evaluate the FPTD of the approximate multi-stage model. This can apply to any nonlinear drift and boundaries.

We show this case via a GDDM with a sinusoidal drift

$$\mu(t) = \frac{1}{2} \sin t,$$

constant diffusion  $\sigma = 1$ , and boundaries

$$u(t) = 2e^{-(t/5)^3}, \quad \ell(t) = -2e^{-(t/5)^3}$$

starting at  $x_0 = -0.5$ . The upper boundary  $u(t)$  is the survival function of a Weibull(5,3) distribution, and  $\ell(t)$  is its reflection about the  $t$ -axis. The particular choice of a Weibull distribution follows relevant examples from prior work [18].

The original boundaries, and the transformed boundaries with their piecewise linear approximations are shown in Figure 6a and Figure 6b, respectively. The computed approximate FPTDs and the histogram consisting of 50,000 samples are displayed in Figure 6c. The approximate FPTD and the histogram agree well.

To quantitatively justify the approximation, we conduct a one-sample Kolmogorov-Smirnov (KS) test. The null hypothesis  $H_0$  is that the sampled first passage

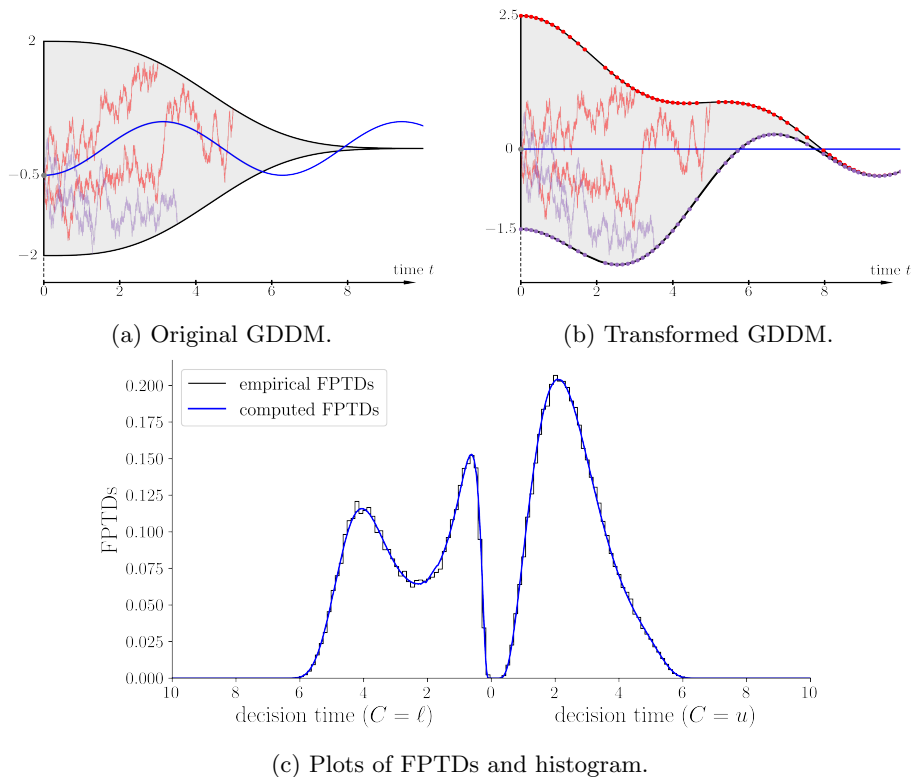


Figure 6: Example 5.2: a GDDM with sinusoidal drift and Weibull survival boundaries. (a) and (b) illustrate the GDDM before and after transformation. The expected value of the process (blue curves) is transformed from a sinusoidal function to a constant zero. In (b), red dots on the upper boundary and purple dots on the lower boundary indicate selected interpolation points for approximating the respective boundaries as piecewise linear functions. (c) displays first passage times: those on the upper boundary appear on the positive  $t$ -axis, while those on the lower boundary appear on the negative  $t$ -axis, forming a valid probability density function.

time data are distributed according to the computed approximate FPTDs. As shown in Table 1a, the KS test does not suggest rejecting  $H_0$  even for sample sizes as large as 100,000. Even though our method of simulating first passage times introduces discretization errors, we believe that these results demonstrate the high accuracy of the FPTD approximation.

### 5.3 FPTDs for Ornstein-Uhlenbeck Models

Consider the Ornstein-Uhlenbeck model in equation (18) with boundaries  $u(t)$  and  $\ell(t)$ . According to the transformation given in Section 4.5, the transformed

#Data	10000	20000	50000	100000
<i>p</i> -value	0.778	0.703	0.498	0.499

(a) Example 5.2: a GDDM with sinusoidal drift and Weibull survival boundaries

#Data	10000	20000	50000	100000
<i>p</i> -value	0.449	0.473	0.179	0.357

(b) Example 5.3: an Ornstein-Uhlenbeck model

Table 1: Results of the one-sample Kolmogorov-Smirnov tests for different data sizes.

boundaries are given by

$$\begin{aligned}\tilde{u}(s) &= \frac{1}{\sigma} \left( u \left( \frac{1}{2\theta} \log(1 + 2\theta s) \right) \sqrt{1 + 2\theta s} - \lambda \sqrt{1 + 2\theta s} + \lambda \right) \\ \tilde{\ell}(s) &= \frac{1}{\sigma} \left( \ell \left( \frac{1}{2\theta} \log(1 + 2\theta s) \right) \sqrt{1 + 2\theta s} - \lambda \sqrt{1 + 2\theta s} + \lambda \right)\end{aligned}$$

We illustrate this case with an example that uses random initial condition  $X(0) \sim \text{Beta}(10, 25)$ . We set the model parameters as  $\theta = 1, \mu = 1.5, \sigma = 2$ , and the original boundaries to be

$$u(t) = 2e^{-(t/2)^3}, \quad \ell(t) = -2e^{-(t/2)^3}$$

We follow the procedures described in Section 4.5: interpolate the transformed boundaries sufficiently fine, compute the approximate transformed FPTDs by Algorithm 1, and obtain the original FPTDs by relation (14). Plots of the FPTDs and statistical tests results are shown in Figure 7 and Table 1b, respectively. From the results we conclude that our method effectively computes the FPTDs of the O-U model (18).

## 5.4 Statistical Computing for aDDMs

In the following examples, we show the effectiveness and efficiency of our method for computing the likelihood and inferring parameters for aDDMs. The aDDM incorporates visual attention as a key factor underlying the decision process behind simple choice behavior. It adjusts the drift rate  $\mu(t)$  based on instantaneous attention within a given experiment trial, adopting values  $\mu_1$  or  $\mu_2$  depending on whether the participant fixates on choice options A or B at time  $t$ . Specifically, if we let  $V(t)$  be the process taking values in  $\{A, B\}$  representing the participant’s visual fixation at time  $t$ , then the aDDM corresponds to the

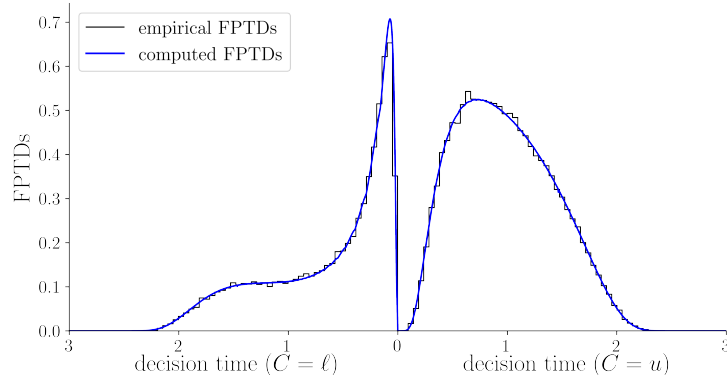


Figure 7: Plots of FPTDs and histogram for Example 5.3: an Ornstein-Uhlenbeck model. First passage times on the upper boundary are displayed on the positive  $t$ -axis and those on the lower boundary are displayed on the negative  $t$ -axis so that the whole plot is a valid probability density function.

following SDE (conditioned on  $V$ ),

$$dX(t) = A(V(t)) dt + \sigma dW(t),$$

$$\text{where } A(v) = \begin{cases} \mu_1 & \text{if } v = \text{A}, \\ \mu_2 & \text{if } v = \text{B}. \end{cases} \quad (20)$$

Note that  $\mu(t) = A(V(t))$  is a piecewise constant function as in the multistage model of Section 4.3, but that it will generally be different on each experimental trial, since a participant's visual fixation process will generally be different on each trial.

In an experimental setting, a participant's fixation trajectory  $V(t)$  is captured using an eye-tracker and can be viewed as a known covariate. Because the fixations drive time-varying drift functions, the configuration  $\Xi$  of the GDDM will be different on each experimental trial. Letting  $\Xi_i$  denote the configuration on the  $i$ -th trial and recalling that  $\Xi_i$  depends on unknown parameters  $\theta$ , such as  $\mu_1$  and  $\mu_2$ , that are shared by all trials and on the known visual fixation trajectory, say  $V_i(t)$ , for the subject's  $i$ -th trial, the likelihood of  $\theta$  is

$$\mathcal{L}_{\text{aDDM}}(\theta \mid \{(\tau_i, C_i)\}_{i=1}^n) = \prod_{i=1}^n f(\tau_i, C_i \mid \Xi_i). \quad (21)$$

Here, we simulate a collection of  $n = 50000$  visual fixation trajectories  $(V_i)_{i=1}^n$  and the corresponding dataset  $((\tau_i, C_i))_{i=1}^n$  from a prescribed aDDM model with alternating drifts  $\mu_1, \mu_2$ , constant diffusion  $\sigma = 1$  and symmetric linear collapsing boundaries

$$u(t) = a - bt, \quad \ell(t) = -a + bt$$

starting at  $x_0 \in (-a, a)$ . The fixation trajectory  $V_i(t)$  on the  $i$ -th trial was sampled from a gamma process to mimic the switching of attention in psychological experiments. The average number of fixations per trial in our simulation was 5.86.

#### 5.4.1 Likelihoods for aDDM given a Dataset

We evaluate the performance of Algorithm 1 for computing likelihoods of the parameters given the dataset  $((\tau_i, C_i))_{i=1}^n$ . The speed of our methods is compared with PyDDM [57], a prominent, widely applied library which serves as a benchmark on speed for the KFE approach (Section 3). When using PyDDM, we chose the finite difference discretization parameters ( $\Delta t = 0.001, \Delta x = 0.001$ ) to be sufficiently small so that the single-trial FPTDs are visually indistinguishable from our solution.

Methods	Time(s)
Algorithm 1 (1 thread)	5.113
Algorithm 1 (8 threads)	0.682
Algorithm 1 (32 threads)	0.275
KFE (1 thread)	17561.83

Table 2: Average times to evaluate the aDDM likelihood in equation (21): Algorithm 1 versus KFE as implemented in PyDDM. Times are average CPU times of 10 repeated evaluations on an AMD EPYC 9684X Processor.

Table 2 shows that our method outperforms the KFE method by more than *three orders of magnitude*. Moreover, our method can easily be further accelerated with parallelization. The speedup of our method for aDDMs largely stems from its ability to progress in large time steps aligned with saccade times, leading to extremely fast single trial computation speed. In contrast, the KFE method requires a much smaller time discretization step to achieve similar accuracy. The accurate analytical formulas in equations (6)–(8) and the high-order efficient quadrature rules in equation (23) in the Appendix further contribute to the method’s speed as they are more accurate than the Crank-Nicolson scheme used in PyDDM.

#### 5.4.2 Statistical Inference of aDDM Parameters

Here we conduct a parameter recovery study for the parameters  $\theta = (\mu_1, \mu_2, a, b, x_0)$  using the maximum likelihood estimator (MLE):

$$\hat{\theta}_n^{\text{MLE}} = \underset{\theta}{\operatorname{argmax}} \mathcal{L}_{\text{aDDM}}(\theta \mid \{(\tau_i, C_i)\}_{i=1}^n) = \underset{\theta}{\operatorname{argmax}} \prod_{i=1}^n f(\tau_i, C_i \mid \Xi_i)$$



We use Algorithm 1 to evaluate the likelihood and the trust region method for optimization. The true and estimated parameters are shown in Table 3 along with component-wise nonparametric pivotal bootstrap confidence intervals.

	True	Estimated	95% CI
$\mu_1$	1.0	0.999	[0.985, 1.015]
$\mu_2$	-0.8	-0.805	[-0.820, -0.790]
$a$	2.1	2.105	[2.093, 2.116]
$b$	0.3	0.303	[0.298, 0.306]
$x_0$	-0.2	-0.197	[-0.209, -0.186]

Table 3: The true and estimated parameters of the aDDM with component-wise nonparametric pivotal bootstrap confidence intervals (based on 1000 bootstrap resamples). All the true parameters fall in their 95% confidence intervals.

Numerical optimization using our method takes on the order of 1 minute with 32 threads, achievable even on a standard desktop computer. In contrast, as it takes almost 5 hours to perform just a single likelihood evaluation using the KFE approach, the numerical optimization would take days or more likely weeks. This illustrates that our method enables fast and accurate parameter recovery.

## 6 Discussion

In this paper, we propose a novel numerical method for computing the first passage time densities (FPTDs), non-passage densities (NPDs), and non-passage probabilities (NPPs) of a general class of drift diffusion models (DDMs) with two time-dependent boundaries. We utilize analytical formulas for certain single-stage models, which are then flexibly combined via numerical quadrature to accommodate a multi-stage framework. We then generalize to prominent, but previously computationally-intractable models in cognitive science [35, 34] and beyond. Our method beats current alternatives by over three orders of magnitude on speed of execution in relevant application scenarios, while maintaining desired accuracy, as shown in Section 5.4.

The benefits over existing approaches are especially notable for the likelihood computation of GDDMs with trial-specific dynamical covariates such as the attentional DDM (aDDM). Despite strong scientific interest, applications of aDDMs have been constrained by computational challenges. Current approaches to inference in aDDMs are based on replacing the aDDM with the gaze-weighted linear accumulator model (GLAM) [38, 40]. The GLAM replaces the time-varying drift rate  $\mu(t)$  in a single trial of the aDDM with the constant drift rate  $\tau^{-1} \int_0^\tau \mu(t) dt$  that is simply the temporal average of the aDDM drift rate on that trial. Although the GLAM enables fast parameter inference using analytic formulas or simulation-based inference (SBI), it is not a well-specified

statistical model, since the drift rate on a trial depends on the decision time on that trial. In parallel work [37], we show that maximum likelihood estimators based on the GLAM likelihood are not consistent for the corresponding aDDM parameters. This further illustrates the importance of developing practical computational tools for the complex GDDMs of interest in cognitive psychology and other fields.

Our focus here is fast likelihood evaluation. For statistical inference it is often useful to also have likelihood gradients. Since the quadrature points used in our implementation of Algorithm 1 are fixed, the algorithm is inherently end-to-end differentiable by automatic differentiation software. In future work we hope to implement Algorithm 1 in an automatic differentiation package such as JAX [8] to allow the use of gradient-based statistical inference methods, such as gradient descent for maximum likelihood estimation and Hamiltonian Monte Carlo for Bayesian inference. Strategies like GPU parallelization and parallel numerical integration could be used to gain even further speed-ups, which might be important in practice when using MCMC for inference in large hierarchical Bayesian models with GDDM likelihoods.

Our approach for multi-stage approximation should be generalizable to broader classes of SDEs than the ones considered here if they admit analytic formulas for FPTDs and NPDs in simple cases and if they have the appropriate Markov structure. If analytic formulas cannot be found, the multistage approximation might still be useful if accurate approximations of single-stage FPTDs and NPDs can be constructed by other methods, such as SBI.

There are several important mathematical questions that we leave for future work relating to regularity conditions for the existence of FPTDs, regularity conditions for the convergence of approximate multistage FPTDs under increasingly fine partitioning, and accuracy of numerical approximations for infinite series truncation, piecewise linear approximation of boundaries, and numerical quadrature. Despite these unresolved issues we believe our algorithms will find immediate use in the psychological and cognitive sciences and will improve the state-of-the-art for statistical inference of GDDMs.

## Acknowledgment

This work was funded by National Institute of Mental Health grants P50 MH119467-01 and P50 MH106435-06A1, Office of Naval Research MURI Award N00014-23-1-2792, and was additionally supported by the Brainstorm Program at the Robert J. and Nancy D. Carney Institute for Brain Science.

## References

- [1] Luigi Acerbi and Wei Ji Ma. Practical Bayesian optimization for model fitting with Bayesian adaptive direct search. *Advances in neural information processing systems*, 30, 2017.
- [2] Todd W Anderson. A modification of the sequential probability ratio test to reduce the sample size. *The Annals of Mathematical Statistics*, pages 165–197, 1960.
- [3] Mark A Beaumont, Wenyang Zhang, and David J Balding. Approximate Bayesian computation in population genetics. *Genetics*, 162(4):2025–2035, 2002.
- [4] Stefan Behnel, Robert Bradshaw, Craig Citro, Lisandro Dalcin, Dag Sverre Seljebotn, and Kurt Smith. Cython: The best of both worlds. *Computing in Science & Engineering*, 13(2):31–39, 2011.
- [5] Rabindra Nath Bhattacharya and Edward C Waymire. *Random walk, Brownian motion, and martingales*. Springer, 2021.
- [6] Steven P Blurton, Miriam Kesselmeier, and Matthias Gondan. Fast and accurate calculations for cumulative first-passage time distributions in Wiener diffusion models. *Journal of Mathematical Psychology*, 56(6):470–475, 2012.
- [7] Jan Boelts, Jan-Matthis Lueckmann, Richard Gao, and Jakob H Macke. Flexible and efficient simulation-based inference for models of decision-making. *Elife*, 11:e77220, 2022.
- [8] James Bradbury, Roy Frostig, Peter Hawkins, Matthew James Johnson, Chris Leary, Dougal Maclaurin, George Necula, Adam Paszke, Jake VanderPlas, Skye Wanderman-Milne, and Qiao Zhang. JAX: composable transformations of Python+NumPy programs, 2018.
- [9] Bingni W. Brunton, Matthew M. Botvinick, and Carlos D. Brody. Rats and humans can optimally accumulate evidence for decision-making. *Science*, 340(6128):95–98, April 2013.
- [10] ID1401986 Cherkasov. On the transformation of the diffusion process to a Wiener process. *Theory of Probability & Its Applications*, 2(3):373–377, 1957.
- [11] Kyle Cranmer, Johann Brehmer, and Gilles Louppe. The frontier of simulation-based inference. *Proceedings of the National Academy of Sciences*, 117(48):30055–30062, 2020.
- [12] Carl De Boor and Carl De Boor. *A practical guide to splines*, volume 27. Springer New York, 1978.

- [13] Adele Diederich and Jerome R Busemeyer. Simple matrix methods for analyzing diffusion models of choice probability, choice response time, and simple response time. *Journal of Mathematical Psychology*, 47(3):304–322, 2003.
- [14] Peter J Diggle and Richard J Gratton. Monte carlo methods of inference for implicit statistical models. *Journal of the Royal Statistical Society Series B: Statistical Methodology*, 46(2):193–212, 1984.
- [15] Takahiro Doi, Yunshu Fan, Joshua I Gold, and Long Ding. The caudate nucleus contributes causally to decisions that balance reward and uncertain visual information. *ELife*, 9:e56694, 2020.
- [16] Joseph L Doob. The Brownian movement and stochastic equations. *Annals of Mathematics*, 43(2):351–369, 1942.
- [17] Alexander Fengler, Krishn Bera, Mads L. Pedersen, and Michael J. Frank. Beyond drift diffusion models: Fitting a broad class of decision and reinforcement learning models with hddm. *Journal of Cognitive Neuroscience*, 34(10):1780–1805, 2022.
- [18] Alexander Fengler, Lakshmi N Govindarajan, Tony Chen, and Michael J Frank. Likelihood approximation networks (lans) for fast inference of simulation models in cognitive neuroscience. *Elife*, 10:e65074, 2021.
- [19] Alexander Fengler, Paul Xu, Omar Aisulu, Krishn Bera, and Michael J Frank. Hssm: A generalized toolbox for hierarchical Bayesian estimation of computational models in cognitive neuroscience. Manuscript in preparation, 2025.
- [20] Brooks Ferebee. The tangent approximation to one-sided Brownian exit densities. *Zeitschrift für Wahrscheinlichkeitstheorie und verwandte Gebiete*, 61(3):309–326, 1982.
- [21] Michael J Frank, Chris Gagne, Erika Nyhus, Sean Masters, Thomas V Wiecki, James F Cavanagh, and David Badre. fmri and eeg predictors of dynamic decision parameters during human reinforcement learning. *Journal of Neuroscience*, 35(2):485–494, 2015.
- [22] Crispin W Gardiner. Handbook of stochastic methods for physics, chemistry and the natural sciences. *Springer series in synergetics*, 1985.
- [23] Paul Glasserman. *Monte Carlo methods in financial engineering*, volume 53. Springer, 2004.
- [24] Emmanuel Gobet. Weak approximation of killed diffusion using euler schemes. *Stochastic processes and their applications*, 87(2):167–197, 2000.
- [25] Emmanuel Gobet and Stéphane Menozzi. Stopped diffusion processes: boundary corrections and overshoot. *Stochastic Processes and Their Applications*, 120(2):130–162, 2010.

- [26] Matthias Gondan, Steven P Blurton, and Miriam Kesselmeier. Even faster and even more accurate first-passage time densities and distributions for the Wiener diffusion model. *Journal of Mathematical Psychology*, 60:20–22, 2014.
- [27] Ian J. Goodfellow, Yoshua Bengio, and Aaron Courville. *Deep Learning*. MIT Press, Cambridge, MA, USA, 2016. <http://www.deeplearningbook.org>.
- [28] WJ Hall. The distribution of Brownian motion on linear stopping boundaries. *Sequential analysis*, 16(4):345–352, 1997.
- [29] Samuel Herrmann and Cristina Zucca. Exact simulation of first exit times for one-dimensional diffusion processes. *ESAIM: Mathematical Modelling and Numerical Analysis*, 54(3):811–844, 2020.
- [30] Samuel Herrmann and Cristina Zucca. Exact simulation of diffusion first exit times: algorithm acceleration. *Journal of Machine Learning Research*, 23(138):1–20, 2022.
- [31] Tomoyuki Ichiba and Constantinos Kardaras. Efficient estimation of one-dimensional diffusion first passage time densities via monte carlo simulation. *Journal of applied probability*, 48(3):699–712, 2011.
- [32] Ioannis Karatzas and Steven Shreve. *Brownian motion and stochastic calculus*, volume 113. springer, 2014.
- [33] Andrei Kolmogoroff. Über die analytischen methoden in der wahrrscheinlichkeitsrechnung. *Mathematische Annalen*, 104:415–458, 1931.
- [34] Ian Krajbich, Carrie Armel, and Antonio Rangel. Visual fixations and the computation and comparison of value in simple choice. *Nature neuroscience*, 13(10):1292–1298, 2010.
- [35] Ian Krajbich, Dingchao Lu, Colin Camerer, and Antonio Rangel. The attentional drift-diffusion model extends to simple purchasing decisions. *Frontiers in psychology*, 3:193, 2012.
- [36] X Sheldon Lin. Double barrier hitting time distributions with applications to exotic options. *Insurance: Mathematics and Economics*, 23(1):45–58, 1998.
- [37] Sicheng Liu, Alexander Fengler, Michael J Frank, and Matthew T Harrison. A simple example that gaze-weighted linear accumulator model is inconsistent for estimating drift in drift-diffusion models. Manuscript in preparation, 2025.
- [38] Gaia Lombardi and Todd Hare. Piecewise constant averaging methods allow for fast and accurate hierarchical Bayesian estimation of drift diffusion models with time-varying evidence accumulation rates, Oct 2021.

- [39] Ralf Metzler, Sidney Redner, and Gleb Oshanin. *First-passage phenomena and their applications*, volume 35. World Scientific, 2014.
- [40] Felix Molter, Armin W Thomas, Hauke R Heekeren, and Peter NC Mohr. Glambox: A python toolbox for investigating the association between gaze allocation and decision behaviour. *PloS one*, 14(12):e0226428, 2019.
- [41] Daniel J Navarro and Ian G Fuss. Fast and accurate calculations for first-passage times in Wiener diffusion models. *Journal of mathematical psychology*, 53(4):222–230, 2009.
- [42] Alex Novikov, Volf Frishling, and Nino Kordzakhia. Approximations of boundary crossing probabilities for a Brownian motion. *Journal of Applied Probability*, 36(4):1019–1030, 1999.
- [43] Liam Paninski, Adrian Haith, and Gabor Szirtes. Integral equation methods for computing likelihoods and their derivatives in the stochastic integrate-and-fire model. *Journal of Computational Neuroscience*, 24:69–79, 2008.
- [44] George Papamakarios, David Sterratt, and Iain Murray. Sequential neural likelihood: Fast likelihood-free inference with autoregressive flows. In *The 22nd International Conference on Artificial Intelligence and Statistics*, pages 837–848. PMLR, 2019.
- [45] Pierre Patie and Chantal Winter. First exit time probability for multidimensional diffusions: A pde-based approach. *Journal of computational and applied mathematics*, 222(1):42–53, 2008.
- [46] Goran Peskir. On integral equations arising in the first-passage problem for Brownian motion. *Journal of Integral Equations and Applications*, 14(4):397–423, 2002.
- [47] Klaus Pötzelberger and Liqun Wang. Boundary crossing probability for Brownian motion. *Journal of applied probability*, 38(1):152–164, 2001.
- [48] Stefan T Radev, Marvin Schmitt, Valentin Pratz, Umberto Picchini, Ullrich Köthe, and Paul-Christian Bürkner. Jana: Jointly amortized neural approximation of complex Bayesian models. In *Uncertainty in Artificial Intelligence*, pages 1695–1706. PMLR, 2023.
- [49] Roger Ratcliff. A theory of memory retrieval. *Psychological review*, 85(2):59, 1978.
- [50] Roger Ratcliff and Gail McKoon. The diffusion decision model: theory and data for two-choice decision tasks. *Neural computation*, 20(4):873–922, 2008.
- [51] Roger Ratcliff and Francis Tuerlinckx. Estimating parameters of the diffusion model: Approaches to dealing with contaminant reaction times and parameter variability. *Psychonomic bulletin & review*, 9(3):438–481, 2002.

- [52] LM Ricciardi and S Sato. A note on the evaluation of first-passage-time probability densities. *Journal of Applied Probability*, 20(1):197–201, 1983.
- [53] Luigi M Ricciardi. On the transformation of diffusion processes into the Wiener process. *Journal of Mathematical Analysis and Applications*, 54(1):185–199, 1976.
- [54] Thomas Richter, Rolf Ulrich, and Markus Janczyk. Diffusion models with time-dependent parameters: An analysis of computational effort and accuracy of different numerical methods. *Journal of Mathematical Psychology*, 114:102756, 2023.
- [55] Donald B Rubin. Bayesianly justifiable and relevant frequency calculations for the applied statistician. *The Annals of Statistics*, pages 1151–1172, 1984.
- [56] Timothy Sauer. *Numerical analysis*. Addison-Wesley Publishing Company, 2011.
- [57] Maxwell Shinn, Norman H Lam, and John D Murray. A flexible framework for simulating and fitting generalized drift-diffusion models. *ELife*, 9:e56938, 2020.
- [58] Philip L Smith. Stochastic dynamic models of response time and accuracy: A foundational primer. *Journal of mathematical psychology*, 44(3):408–463, 2000.
- [59] Philip L Smith and Roger Ratcliff. Modeling evidence accumulation decision processes using integral equations: Urgency-gating and collapsing boundaries. *Psychological review*, 129(2):235, 2022.
- [60] Vaibhav Srivastava, Samuel F Feng, Jonathan D Cohen, Naomi Ehrich Leonard, and Amitai Shenhav. A martingale analysis of first passage times of time-dependent Wiener diffusion models. *Journal of mathematical psychology*, 77:94–110, 2017.
- [61] Volker Strassen et al. Almost sure behavior of sums of independent random variables and martingales. In *Proceedings of the Fifth Berkeley Symposium on Mathematical Statistics and Probability*, volume 2, pages 315–343. Univ. of California Press Berkeley, CA, 1967.
- [62] James William Thomas. *Numerical partial differential equations: finite difference methods*, volume 22. Springer Science & Business Media, 2013.
- [63] Francis Tuerlinckx, Eric Maris, Roger Ratcliff, and Paul De Boeck. A comparison of four methods for simulating the diffusion process. *Behavior Research Methods, Instruments, & Computers*, 33:443–456, 2001.
- [64] Marius Usher and James L McClelland. The time course of perceptual choice: the leaky, competing accumulator model. *Psychological review*, 108(3):550, 2001.

- [65] Andreas Voss and Jochen Voss. Fast-dm: A free program for efficient diffusion model analysis. *Behavior research methods*, 39(4):767–775, 2007.
- [66] Andreas Voss and Jochen Voss. A fast numerical algorithm for the estimation of diffusion model parameters. *Journal of Mathematical Psychology*, 52(1):1–9, 2008.
- [67] Liqun Wang and Klaus Pötzelberger. Boundary crossing probability for Brownian motion and general boundaries. *Journal of Applied Probability*, 34(1):54–65, 1997.
- [68] Liqun Wang and Klaus Pötzelberger. Crossing probabilities for diffusion processes with piecewise continuous boundaries. *Methodology and Computing in Applied Probability*, 9:21–40, 2007.
- [69] E Weinan, Tiejun Li, and Eric Vanden-Eijnden. *Applied stochastic analysis*, volume 199. American Mathematical Soc., 2021.
- [70] Thomas V Wiecki, Imri Sofer, and Michael J Frank. Hddm: Hierarchical Bayesian estimation of the drift-diffusion model in python. *Frontiers in neuroinformatics*, 7:14, 2013.
- [71] Christopher KI Williams and Carl Edward Rasmussen. *Gaussian processes for machine learning*, volume 2. MIT press Cambridge, MA, 2006.
- [72] Michael M Yartsev, Timothy D Hanks, Alice Misun Yoon, and Carlos D Brody. Causal contribution and dynamical encoding in the striatum during evidence accumulation. *Elife*, 7:e34929, 2018.



## A Proof of Almost Sure Convergence of First Passage Times under Refined Boundary Approximations

In this section, we establish the following result, which serves as the mathematical foundation of approximating the first passage times on curved boundaries by first passage times on their piece-wise linear approximations, as described in Section 4.4. Specifically, we consider the simplified setting where the diffusion process is a Brownian motion with a single upper boundary.

**Theorem A.1.** *Let  $W(t)$  be a one-dimensional Brownian motion on a probability space  $(\Omega, \mathcal{F}, \mathbb{P})$ , and let  $u(t)$  be a function on  $[0, \infty)$  that is Hölder continuous with exponent  $1/2$ , satisfying  $u(0) > 0$ . Suppose that a sequence of continuous functions  $\{u_n\}$  converges uniformly to  $u$  on compact subsets of  $[0, \infty)$ . Define the first passage times  $\tau, \tau_n$  as*

$$\begin{aligned}\tau &= \inf\{t > 0 : W(t) \geq u(t)\} \\ \tau_n &= \inf\{t > 0 : W(t) \geq u_n(t)\}\end{aligned}$$

Then,  $\tau_n$  converges to  $\tau$  almost surely.

*Proof of Theorem A.1.* Define

$$\begin{aligned}\tau^* &= \inf\{t > 0 : W(t) > u(t)\} \\ \tau_n^* &= \inf\{t > 0 : W(t) > u_n(t)\}\end{aligned}$$

We prove the desired result in three steps.

- $\liminf_{n \rightarrow \infty} \tau_n \geq \tau$ .

Fix  $\omega \in \Omega$ . For any  $\epsilon > 0$ , the function  $t \mapsto u(t) - W(t)$  is continuous and attain its minimum  $\delta = \delta(\epsilon) > 0$  on  $[0, \tau - \epsilon]$ , i.e.,  $W(t) < u(t) - \delta$  when  $t \leq \tau - \epsilon$ . Since  $u_n \rightarrow u$  uniformly on  $[0, \tau - \epsilon]$ , there exists  $N = N(\delta) = N(\epsilon)$  such that for all  $n \geq N$  we have  $u_n(t) > u(t) - \delta > W(t)$  for  $t < \tau - \epsilon$ . Thus, we have that for all  $t < \tau - \epsilon$  and  $n \geq N$ ,  $W(t) < u_n(t)$ . This implies  $\tau_n \geq \tau - \epsilon$  for  $n \geq N$ . Taking  $\epsilon \rightarrow 0$  gives  $\liminf_{n \rightarrow \infty} \tau_n \geq \tau$ .

- $\limsup_{n \rightarrow \infty} \tau_n^* \leq \tau^*$ .

Fix  $\omega \in \Omega$ . By the definition of  $\tau^*$ , we know that for any  $\epsilon > 0$ , there exists  $t_\epsilon \in (\tau^*, \tau^* + \epsilon)$  and  $\delta > 0$ , such that  $W(t_\epsilon) > u(t_\epsilon) + \delta$ . Since  $u_n(t_\epsilon) \rightarrow u(t_\epsilon)$ , there exists  $N = N(\delta) = N(\epsilon)$  such that for all  $n \geq N$  we have  $u_n(t_\epsilon) < u(t_\epsilon) + \delta < W(t_\epsilon)$ . Thus, there exists a  $t_\epsilon \in (\tau^*, \tau^* + \epsilon)$  such that  $u_n(t_\epsilon) < W(t_\epsilon)$  for  $n \geq N$ . This implies  $\tau_n^* \leq \tau^* + \epsilon$  for  $n \geq N$ . Taking  $\epsilon \rightarrow 0$  gives  $\limsup_{n \rightarrow \infty} \tau_n^* \leq \tau^*$ . Hence  $\limsup_{n \rightarrow \infty} \tau_n^* \leq \tau^*$ .

- $\tau = \tau^*$  a.s.

The inequality  $\tau \leq \tau^*$  is immediate, so it suffices to show that  $\mathbb{P}(\tau < \tau^*) = 0$ . Without loss of generality, we assume that  $\tau$  is almost surely finite, since for any  $\omega$  where  $\tau(\omega) = \infty$ , we trivially have  $\tau(\omega) = \tau^*(\omega) = \infty$ .

Take  $\omega$  where  $\tau(\omega) < \tau^*(\omega)$ , then there exist  $\delta > 0$  such that  $W(t) \leq u(t)$  for  $t \in (\tau, \tau + \delta)$ . By the strong Markov property of  $W$ , we know that  $B(s) = W(s + \tau) - W(\tau)$  is also a Brownian motion. Let  $C$  be the Hölder  $C^{0,1/2}$  semi-norm of  $u$ , then we have  $u(t) \leq u(\tau) + C(t - \tau)^{1/2}$  for  $t > \tau$ . Hence, we have

$$W(\tau) + B(s) = W(s + \tau) \leq u(s + \tau) \leq u(\tau) + Cs^{1/2}$$

when  $s \in (0, \delta)$ . By the continuity of  $W$  and  $u$  we have  $W(\tau) = u(\tau)$ , so  $B(s) \leq Cs^{1/2}$  for  $s \in (0, \delta)$ .

However, this would imply

$$\limsup_{s \rightarrow 0^+} \frac{B(s)}{\sqrt{2s \log \log(1/s)}} \leq \limsup_{s \rightarrow 0^+} \frac{C}{\sqrt{2 \log \log(1/s)}} = 0 \quad (22)$$

Yet, the law of the iterated logarithm states that

$$\limsup_{s \rightarrow 0^+} \frac{B(s)}{\sqrt{2s \log \log(1/s)}} = 1 \quad \text{a.s.}$$

so equation (22) holds with probability 0. So  $\mathbb{P}(\tau < \tau^*) = 0$ .

Combining the above results, we obtain

$$\tau \leq \liminf_{n \rightarrow \infty} \tau_n \leq \limsup_{n \rightarrow \infty} \tau_n \leq \limsup_{n \rightarrow \infty} \tau_n^* \leq \tau^*$$

from  $\tau = \tau^*$  a.s., we conclude that  $\lim_{n \rightarrow \infty} \tau_n = \tau$  a.s.. ■

Adopting the notations in Section 4.4 and the footnote in Section 2, the piecewise linear interpolations of the continuous boundaries  $u$  and  $\ell$ , denoted by  $\bar{u}$  and  $\bar{\ell}$  respectively, converge to  $u$  and  $\ell$  uniformly on compact subsets of  $[0, \infty)$  as the interpolation grid is refined (see P35 of [12]). Consequently, we can invoke Theorem A.1 to conclude that the approximate first passage time  $\bar{\tau}_u$  and  $\bar{\tau}_\ell$  converge almost surely to  $\tau_u$  and  $\tau_\ell$  on their respective boundaries. Since  $\bar{\tau} = \bar{\tau}_u \wedge \bar{\tau}_\ell$ ,  $\tau = \tau_u \wedge \tau_\ell$ , it follows that  $\bar{\tau} \rightarrow \tau$  a.s..

## B Transformation of a Diffusion Process to a Brownian Motion

Here, we present the Cherkasov condition as outlined in [53], which provides the necessary and sufficient conditions for the existence of the transformation (13) that converts a diffusion process  $X(t)$  into a Brownian motion.

**Theorem B.1** ([53]). *Let  $X(t)$  be a diffusion process defined on interval  $[0, T_{end}]$  satisfying the SDE (2). If there exists a pair of functions  $c_1(t)$  and  $c_2(t)$  such that*

$$\mu(x, t) = \frac{\frac{\partial}{\partial x} (\sigma^2(x, t))}{4} + \frac{\sigma(x, t)}{2} \left( c_1(t) + \int_0^x \frac{c_2(t) \sigma^2(y, t) + \frac{\partial}{\partial t} (\sigma^2(y, t))}{\sigma^3(y, t)} dy \right)$$

then there exists a coordinate transformation of the form (13) such that  $\psi(X(\gamma^{-1}(s)), \gamma^{-1}(s))$ , the image of  $X(t)$  under this transformation, has the same dynamics with a standard Brownian motion. This transformation is given by

$$s = \gamma(t) = \int_0^t e^{-\int_0^r c_2(z) dz} dr$$

$$w = \psi(x, t) = e^{-\frac{1}{2} \int_0^t c_2(s) ds} \int_0^x \frac{1}{\sigma(y, t)} dy - \frac{1}{2} \int_0^t c_1(r) e^{-\frac{1}{2} \int_0^r c_2(z) dz} dr$$

We take the Ornstein-Uhlenbeck process (18) as an example. Here  $\mu(x, t) = \theta(\lambda - x)$  and  $\sigma(x, t) = \sigma$ , and we can take  $c_1(t) = \frac{2\theta\lambda}{\sigma}$ ,  $c_2(t) = -2\theta$ . Correspondingly, the transformation is given by  $s = \gamma(t) = \frac{e^{2\theta t} - 1}{2\theta}$ ,  $w = \psi(x, t) = \frac{1}{\sigma}(e^{\theta t}x - \lambda e^{\theta t} + \lambda)$ . This is the same as the transformation given in Section 4.5.

## C Detailed Implementation of the Quadrature

The  $m$ -point Gauss-Legendre quadrature is given by

$$\int_a^b f(x) dx \approx \frac{b-a}{2} \sum_{i=1}^m w_i f\left(\frac{b-a}{2}\xi_i + \frac{a+b}{2}\right)$$

$$= \frac{b-a}{2} \mathbf{w}^\top f\left(\frac{b-a}{2}\boldsymbol{\xi} + \frac{a+b}{2}\right)$$
(23)

where  $\mathbf{w} = (w_1, \dots, w_m)^\top$  are the quadrature weights,  $\boldsymbol{\xi} = (\xi_1, \dots, \xi_m)^\top$  are the quadrature points on the reference interval  $[-1, 1]$ . The formula (23) is exact for polynomials of degree up to  $2m - 1$ .  $\mathbf{w}$  and  $\boldsymbol{\xi}$  can be computed by formulas involving Legendre polynomials but are usually tabulated to great accuracy.

To apply formula (23) to our algorithm, at each stage, we only need to track the density at precomputed quadrature points on each vertical boundary. We then proceed to the next stage by computing the transitional density to the quadrature points on the next vertical boundary (see Figure 8). Suppose we use quadrature of order  $m_k$  for integrating in the  $k$ -th stage. The functions in equations (6) and (7) are observed to exhibit a more rapid growth of derivatives compared to those in equation (8), hence the integrand in the final stage is less regular than in the earlier stages. Therefore, we typically employ a higher-order quadrature rule for the integration in the final stage. Specifically, if  $\tau$  is in the  $K$ -th stage we can take  $m_K \geq m_i$  for  $i = 1, \dots, K - 1$  for more efficient computation.

Here, we present Algorithm 1', which incorporates numerical integration via (23) into Algorithm 1. Note that different initial treatments are needed for discrete and continuous  $X(0)$ , as if  $X(0)$  is discrete, we only need to directly use formulas (9), (10) and (11), and there is no need for integration in the first stage. In cases where  $X(0)$  is a mixture of discrete and continuous components, we handle each part accordingly. However, we omit this case in Algorithm 1' for brevity, as its treatment follows naturally from the discrete and continuous

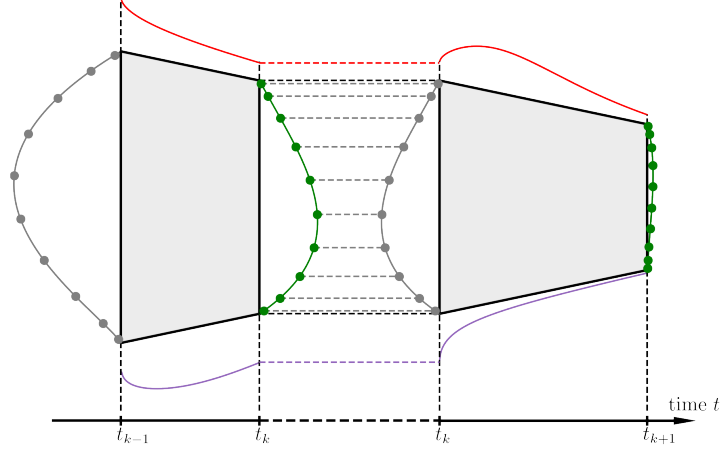


Figure 8: At each vertical boundary between two stages, probability transfer occurs through a set of precomputed quadrature points—green dots on the output boundaries and grey dots on the input boundaries. The function  $q_k$ , evaluated at the quadrature points along the vertical boundary at  $t = t_k$  (denoted as  $\mathbf{q}_k$  in Algorithm 1'), encapsulates the necessary information for integrating over the probability measure of the starting position  $X(t_k)$ , to facilitate computations in the next stage.

cases. In Algorithm 1', we denote the abstract process of acquiring  $\mathbf{w}, \boldsymbol{\xi}$  of order  $m$  as  $\mathbf{w}, \boldsymbol{\xi} \leftarrow \text{gausslegendre}(m)$ , and the symbol  $\odot$  represents the Hadamard (element-wise) product for vectors.

---

**Algorithm 1'**: Sequential likelihood evaluation of a multi-stage GDDM, with Gauss-Legendre quadrature

---

**Input** : A multi-stage model configuration as described in Section 4.3;  
 An observation  $(t, c)$  for  $t_{K-1} < t \leq t_K$  ( $t$  is in the  $K$ -th stage) and  $c \in \{u, \ell\}$  or an observation of “non-response”, in the latter case the number of effective stages  $K$  is set to be  $d + 1$ ;  $q_0$  as the sub-probability “density” of  $X(0)$ .

**Output**:  $f(t, c) = f_c(t)$  for a datum pair  $(t, c)$ , or  $Q$  for “non-response”

```

if  $q_0$  is a pdf then /*  $X(0)$  is continuous */
  |  $\mathbf{w}_0, \boldsymbol{\xi}_0 \leftarrow \text{gausslegendre}(m_0)$ ;
  |  $\mathbf{x}_0 \leftarrow \frac{u(t_0) - \ell(t_0)}{2} \boldsymbol{\xi}_0 + \frac{\ell(t_0) + u(t_0)}{2}$ ;
  |  $\mathbf{q}_0 = q_0(\mathbf{x}_0)$ ;
else if  $q_0 = \sum_{j=1}^J w_{0j} \delta_{x_{0j}}$  then /*  $X(0)$  is discrete */
  |  $\mathbf{w}_0 \leftarrow (w_{01}, \dots, w_{0J})^\top$ ;
  |  $\mathbf{x}_0 \leftarrow (x_{01}, \dots, x_{0J})^\top$ ;
  |  $\mathbf{q}_0 \leftarrow (1, \dots, 1)^\top$ ;
end
for  $k = 1$  to  $K - 1$  do
  |  $\mathbf{w}_k, \boldsymbol{\xi}_k \leftarrow \text{gausslegendre}(m_k)$ ;
  |  $\mathbf{x}_k \leftarrow \frac{u(t_k) - \ell(t_k)}{2} \boldsymbol{\xi}_k + \frac{\ell(t_k) + u(t_k)}{2}$ ;
  |  $\mathbf{P}_k \leftarrow q^{\text{single}}(\mathbf{x}_k; \mu_k, \sigma_k, \mathcal{B}_k, \mathbf{x}_{k-1}^\top)$ ;
  |  $\mathbf{q}_k \leftarrow \mathbf{P}_k(\mathbf{q}_{k-1} \odot \mathbf{w}_{k-1})$ ;
end
if observation is  $(t, c)$  then
  |  $\mathbf{c}_K \leftarrow f_c^{\text{single}}(t - t_{K-1}; \mu_K, \sigma_K, \mathcal{B}_K, \mathbf{x}_{K-1}^\top)$ ;
  |  $f(t, c) \leftarrow \mathbf{c}_K(\mathbf{q}_{K-1} \odot \mathbf{w}_{K-1})$ ;
else if observation is “non-response” then
  |  $Q \leftarrow \mathbf{w}_d^\top \mathbf{q}_d$ 
end

```

---